Implications of longitudinal ridges for the mechanics of ice-free long runout landslides.

Giulia Magnarini[1], Thomas M Mitchell[1], Liran Goren[2], Peter Grindrod[3] and John Browning[4]

[1]Department of Earth Sciences, University College London, London, United Kingdom.

[2]Department of Earth and Environmental Sciences, Ben Gurion University of Negev, Beer-Sheva, Israel.

[3]Natural History Museum, London, United Kingdom.

[4] Department of Structural and Geotechnical Engineering and Department of Mining Engineering, Pontificia Universidad Catholica de Chile.

CORRESPONDING AUTHOR

Giulia Magnarini, *giulia.magnarini.14@ucl.ac.uk*

ABSTRACT

The emplacement mechanisms of long runout landslides across the Solar System and the formation mechanisms of longitudinal ridges associated with their deposits remain subjects of debate. The similarity of longitudinal ridges in martian long runout landslides and terrestrial landslides emplaced on ice suggests that an icy surface could explain both the reduction of friction associated with the deposition of long runout landslides and the development of longitudinal ridges. However, laboratory experiments on rapid granular flows show that ice is not a necessary requirement for the development of longitudinal ridges, which instead may form from convective cells within high-speed flows. These experiments have shown that the wavelength (S) of the ridges is 2-3 times the thickness (T) of the flow, which has also been demonstrated at field scale on

a tens-of-kilometre martian long runout landslide. Here, we present the case study of the 4-km-long, ice-free El Magnifico landslide in Northern Chile which exhibits clear longitudinal ridges, and show for the first time on a terrestrial landslide that the S/T ratio is in agreement with the scaling relationship found for both laboratory rapid granular flows and a previously measured martian long runout landslide. Several outcrops within the landslide allow us to study internal sections of the landslide deposit and their relationship with the longitudinal ridges in order to shed light on the emplacement mechanism. Our observations include interactions without chaotic mixing between different lithologies and the presence of meters-sized blocks that exhibit preserved original bedding discontinuities. We associate these observations with fluctuations in stress, as they are qualitatively similar to numerically modelled rapid granular slides, which were suggested, to some degree, to be associated with acoustic fluidization. Our results suggest that 1) the mechanism responsible for the formation of longitudinal ridges is scale- and environment-independent; 2) while the internal structures observed do not necessarily support a mechanism of convective-style motion, their interpretation could also point to a mechanism of internal deformation of the sliding mass derived from pattern-forming vibrations. Our novel observations and analysis provide important insights for the interpretation of similar features on Earth and Mars and for discerning the underlying mechanisms responsible for the emplacement of long run out landslides.

KEYWORDS

Longitudinal ridges; Long runout landslide; Deposit thickness; Scaling relationship; Emplacement mechanism.

1 INTRODUCTION

Long runout landslides are hypermobile mass-wasting phenomena that are found throughout the Solar System, on planets, moons, and asteroids (Howard, 1973; Lucchitta, 1979; Singer et al., 2012; Schmidt et al.,

2017; e.g., Beddingfield et al., 2019). One key morphological feature that is commonly documented in long runout landslides across the Solar System are distinctive longitudinal ridges that run parallel to the flow direction (Howard, 1973; Lucchitta, 1979; Schmidt et al., 2017; Boyce et al., 2020). In particular, long runout landslides that are tens of kilometres long exhibiting prominent longitudinal ridges constitute one of the dominant landforms of the martian landscape, which has been sculpted by gigantic mass-wasting events throughout its geological history (Quantin et al., 2004b) and on a global scale (Crosta et al., 2018).

The variety of physical and climatic conditions at which long runout landslides form suggests a variety of complex mechanisms that lead to their exceptional behaviour. The high mobility of long runout landslides suggests an apparent reduction of friction during such catastrophic events which has been attributed to a series of velocity-dependent, thermally activated mechanisms operating at the base of the slide (Erismann et al., 1977; Voight and Faust, 1982; Legros et al., 2000; Vardoulakis, 2000; Goren and Aharonov, 2007; Goren et al., 2010; Mitchell et al., 2015; Schmidt et al., 2017; Hu et al., 2018) or to bulk fluidization of the sliding mass (Melosh, 1979; Davies, 1982; Collins and Melosh, 2003; Davies and McSaveney, 2009). Despite the variety of suggested weakening mechanisms, the dominant processes that control the formation mechanism of long runout landslides on planetary bodies, the origin of their acceleration and high velocity, and the origin of the dramatic reduction of friction needed to explain their catastrophic behaviour, remain controversial and unresolved. The morphological features and internal structures of long runout landslides can be used to infer the possible mechanics of emplacement (e.g., Weidinger et al., 2014; Dufresne et al., 2016). As such, many efforts have been made to describe the morphology, the sedimentology and the internal fabric of long runout landslide deposits (e.g., Legros et al., 2000; Shea and van Wyk de Vries, 2008; Dufresne and Davies, 2009; Paguican et al., 2014), in the attempt to clarify the relationship between their development and the mechanisms that take place during their catastrophic emplacements.

Direct observations of terrestrial long runout landslide deposits are crucial in attempting to understand the mechanics of long runout landslides and they represent invaluable information for interpreting similar features on other planetary bodies. For example, on Mars, the presence of longitudinal ridges in long runout landslides has often been associated with the presence of basal ice (De Blasio, 2011), as longitudinal ridges

have been commonly observed on terrestrial landslides that were emplaced over glaciers. However, ice-free laboratory experiments and simulations on instability patterns in rapid granular flows performed by Forterre and Pouliquen (2001) and Borzsonyi et al. (2009) show that longitudinal ridges spontaneously develop from a mechanical instability that emerges from the physics of fast-flowing granular flows, which generates convective, helicoidal cells extending longitudinal to the flow direction. Moreover, it is found that the wavelength of the ridges scales with the thickness of the flow. The same scaling relationship has now been found in a martian long runout landslide, suggesting that such convective cells may be responsible for ridge formation in nature. This is also considered supportive of the hypothesis that ice is not a necessary condition for the formation of longitudinal ridges in long runout landslides (Magnarini et al., 2019).

If convection is responsible for the formation of longitudinal ridges, this would likely be reflected within the internal structure of the landslide deposit. To date, no such observations have been made, due to the inaccessibility of planetary examples, including terrestrial examples on remote glaciers, poorly preserved structures, or lack of convenient outcrops. Here, we examine pronounced examples of longitudinal ridges on a very well preserved ancient long runout landslide in the hyper-arid Atacama desert, Northern Chile. We focus on the morphology and sedimentology of longitudinal ridges of the El Magnifico rock avalanche cluster, whose emplacement could not have been associated with basal ice. The El Magnifico landslide is located on the coastal plain of the northern part of the Atacama Desert, Chile (Figure 1a-c) and it occurred ± 60 kya (Crosta et al., 2017), at a time when ice-free, low-altitude coastal areas and regional hyper-arid conditions were long established (Amundson et al., 2012). The hyper-arid environment of the Atacama region allows exceptional preservation of the geomorphological record over long time scales due to low erosion rates (e.g., Evenstar et al., 2017), representing an ideal site to conduct detailed morphological observations and morphometric analysis of the El Magnifico landslide and its associated longitudinal ridges.

Using satellite and drone high resolution images and elevation models, we conduct morphometric analysis and demonstrate that the relationship between the wavelength of these terrestrial longitudinal ridges and the thickness of the landslide scales in agreement with both planetary studies and laboratory experiments. We also describe the internal structures of the landslide deposit, as observed at a number of available

outcrops, and assess their relationship with longitudinal ridges. We finally combine the results and observations to discuss the implications for the emplacement mechanism of long runout landslides with longitudinal ridges. Our aim is to provide novel terrestrial observations to help the interpretation of similar features on Earth and on Mars.

2 AREA OF STUDY.

The El Magnifico rock avalanche cluster was first reported in detail by Mather et al. (2014). It represents an exemplary well-preserved terrestrial unconfined long runout landslide that comprises 7 lobes (Figure 1e). In this study, we will refer to individual lobes following the numeration, from 1 to 7, as given by Mather et al. (2014). The subdivision was made from remote sensing and field mapping, where 1 represents the first lobe to be emplaced and 7 the last lobe to be emplaced. Using ^{14}C dating of organic material stratigraphically related to the rock avalanche deposit, ^{36}Cl cosmogenic nuclide, and optical stimulated luminescence, Crosta et al. (2017) have dated the rock avalanche cluster to 60 ± 10 kya. Unfortunately, dating uncertainties do not permit attribution of the time interval between the discrete events that generated the lobes.

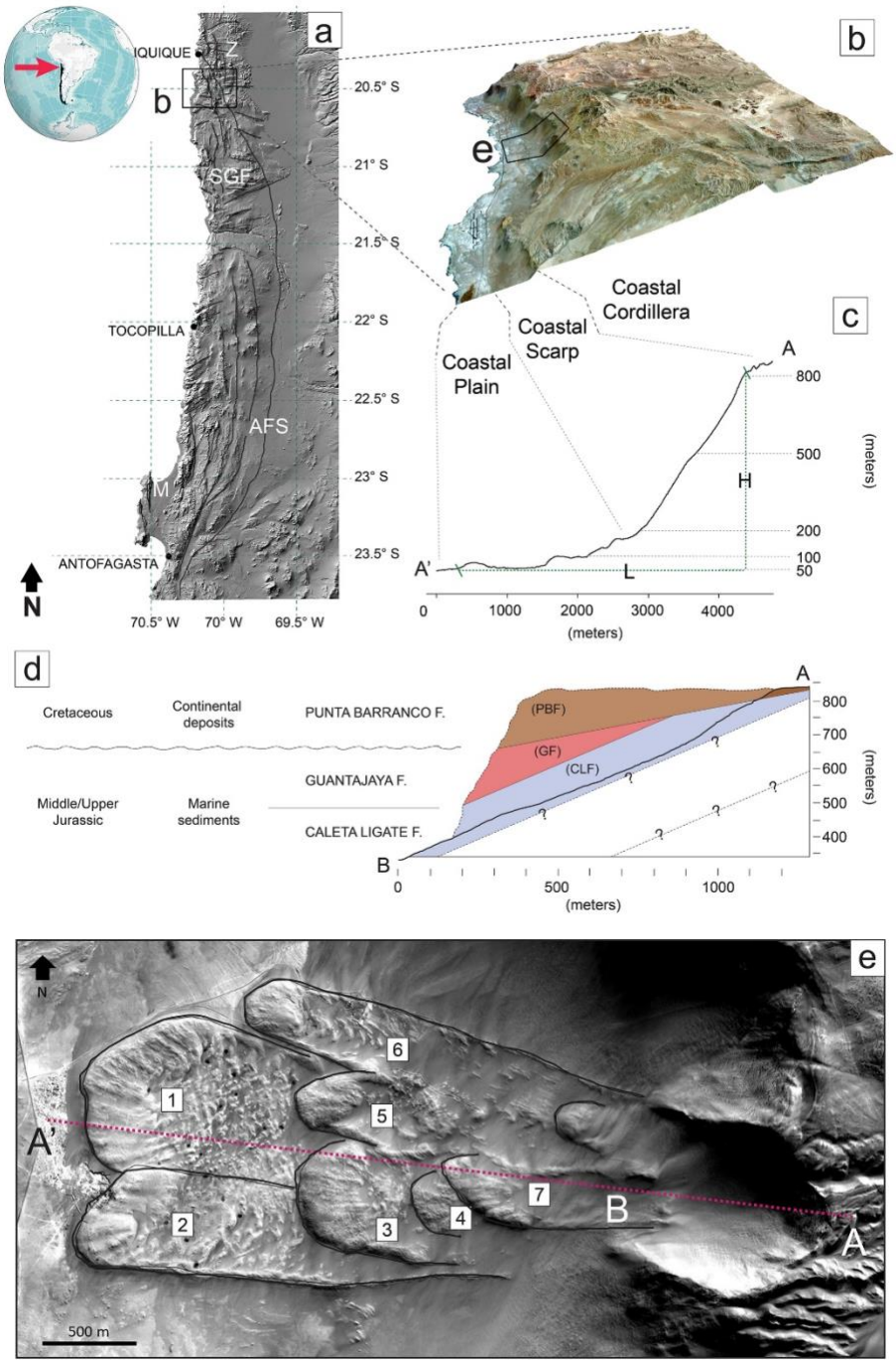

Figure 1 – Area of Study. a) Shaded relief map of northern Chile obtained from the SRTM Global_3 (90m); black lines represent major faults; AFS = Atacama Fault System, M = Mejillones, SGF = Salar Grande Fault. b) Oblique view of the Sentinel multispectral image (Bands R5, G2, B1) overlying the SRTM Global DEM. c) block diagram shows the three physiographic units involved in the study area. d) Reconstructed geological section of the slope prior failure. e) Orthoimage from Pleiades satellites of the El Magnifico landslide cluster; numbers represent the lobes that form the cluster, as given by Mather et al. (2014); Red dotted line shows the location of the topographic profile shown in e.

The landslide cluster is located about 25 km south of Iquique, and originated from the collapse of a portion of the Coastal Cordillera scarp and it has been emplaced on the coastal plain formed by Pleistocene marine terrace deposits (Figure 1a-c). In this area of the Coastal Cordillera, the Jurassic and Cretaceous formations are intruded by andesitic and granodioritic plutons (Novoa, 1970), which are cut by normal faults that follow a N-S trend, E-W-striking reverse faults, and WNW and NNW-striking dextral strike-slip faults (Allmendinger and González, 2010). In particular, the cliff that was affected by the slope failure that generated the El Magnifico landslide is characterized by a sequence of layered sedimentary rock, sandstones and pervasively foliated black to red to yellow siltstones and marls with localized thin levels of gypsum, overlain by conglomerates, through angular unconformity relationship (Figure 1d, Supplementary Material S1). The slope failure has likely exploited bedding discontinuities that dip to the west (Figure 1d); joints, faults and fractures orientation suggest that these cross-cutting planes have affected the shape of the head scarp (Mather et al., 2014). Unfortunately, large areas of the coastal scarp, including the scarp of the El Magnifico landslide, are covered by wind-blown sands, limiting the locations at which outcrops are available. This is also true for locations on the coastal plain, where aeolian deposits locally shroud the landslide deposit, impeding observation of the contact between the deposit and the coastal plain surface.

As read along the median transversal profile A-A' in Figure 1c, the landslide is characterized by an elevation drop (H) of about 750 m. The horizontal runout (L), measured from the highest point of the scarp to the lowest point of the deposit, is about 4 km. This results in a H/L ratio of about 0.2. The lobes that form the rock avalanche cluster have a terminal bulging morphology and a depressed central area (Figure 2a). Besides having distinctive elevations, the terminal and central parts also present distinctive morphologies: the higher-elevation rims exhibit longitudinal ridges, which extend from about 50 to 400 m, whereas lower-elevation central areas exhibit hummocky features (Figure 2c). The depressed-hummocky central areas are bordered by lateral levees, which at times are double-ridged.

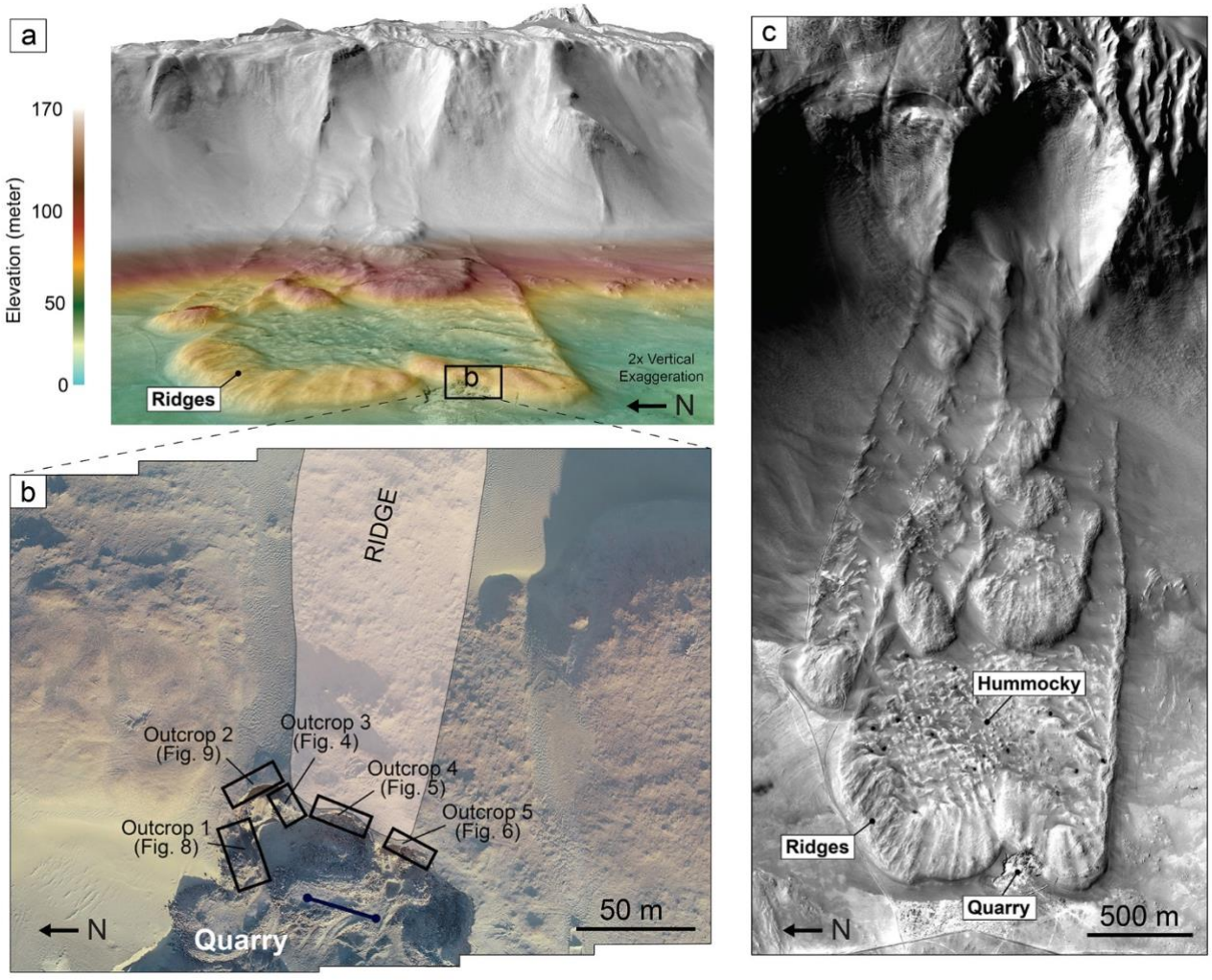

Figure 2 – Oblique view of the El Magnifico landslide cluster. a) Digital elevation model is obtained from Pleiades satellites images; b) nadir-view of the quarry showing the locations of the outcrops discussed in the paper; the location of the ridge cut by the quarry excavation is represented by the light-coloured area; the blue line with round arrowheads represent the location of the outcrop described in Mather et al. (2014) (Anonymous reviewer, personal communication) c) orthorectified image obtained from Pleiades satellite images showing the distinct morphologies of the longitudinal ridges along the terminal lobe rims and the hummocky terrains at the lobes center.

3 SATELLITE AND DRONE PHOTOGRAMMETRY MAPPING.

We used Pleiades Satellite stereo-images (©CNES, 2013, distribution Airbus Defence and Space) to generate a high-resolution Digital Elevation Model (DEM) and orthorectified images (orthoimages) (Table 1) of the area that entirely covers the landslide deposit and its source area, and the adjacent coastal plane surface,

158 using commercial photogrammetry software SOCET GXP from BAE Systems. These image products have been
159 used to reconstruct the surface underneath the landslide deposit by interpolating between topographic
160 contours of the coastal plane directly adjacent the landslide deposit (see Supplementary Material S6), as
161 previously done by other studies (e.g., Quantin et al., 2004a; Conway and Balme, 2014; Magnarini et al.,
162 2019). This reconstructed surface is used to calculate the thickness of the deposit.

163 We conducted two field campaigns at the El Magnifico landslide site, in 2018 and 2019. With the use of
164 drones (DJI Phantom Pro series), we collected nadir images (i.e., camera angle is perpendicular to the ground
165 surface) of the terminal 1.5 km of the deposit, which corresponds to the area that includes lobes 1 and 2
166 (distal lobes), 3 and 5 (middle lobes) (Figure 3a, Table 1). We made use of the mission planner 'Pix4D Capture'
167 app to plan flight routes and image acquisition (see Supplementary Material T1, S3b-c). From this image
168 dataset we made high resolution DEMs and orthophotos using commercial photogrammetry software Agisoft
169 Photoscan (Table 1, Supplementary Material S4). We applied several waypoints using coordinate information
170 of terrain markers easily identifiable on Pleiades-derived orthoimages (Supplementary Material, T2 and S3a).
171 This approach provided consistency between these two different datasets and avoided introducing further
172 error into our landslide deposit thickness calculation (Supplementary Material S5). The DEMs and
173 orthophotos that cover lobes 1, 2, and 3 have been used for morphometric analysis of the longitudinal ridges
174 that appear in the terminal part of the lobes.

175

176

177

178

179

180

181

Table 1 – List of imagery datasets used for this work.

Locality	Data Source	Data Products		Software
		DEM	**Orthoimage**	
Context Area (Figure 1a)	Pleiades Satellites	2 m/px	B+W: 0.5 m/px Colour: 2 m/px	BAE Systems SOCET GXP
Distal Lobes (Figure 3)	Drone	8.22 cm/px	4.11 cm/px	Agisoft Photoscan
Middle Lobes (Figure 3)	Drone	12.4 cm/px	6.19 cm/px	Agisoft Photoscan

4 SCALING RELATIONSHIP BETWEEN THE WAVELRNGTH OF LONGITUDINAL RIDGES AND DEPOSIT THICKNESS.

In this section, we follow the approach used in Magnarini et al. (2019). In ArcGIS, we mapped longitudinal ridges tracing a line corresponding to the crest of each of the ridges (Figure 3a). We conducted the morphometric analysis at lobes 1, 2, and 3, where the ridge morphologies are most prominent. We traced one transverse profile at each of the lobes (Figure 3a) and we measured the distance between the ridges. We then calculated the average spacing between the ridges, which we considered representative of the wavelength of the ridges (S in Table 2).

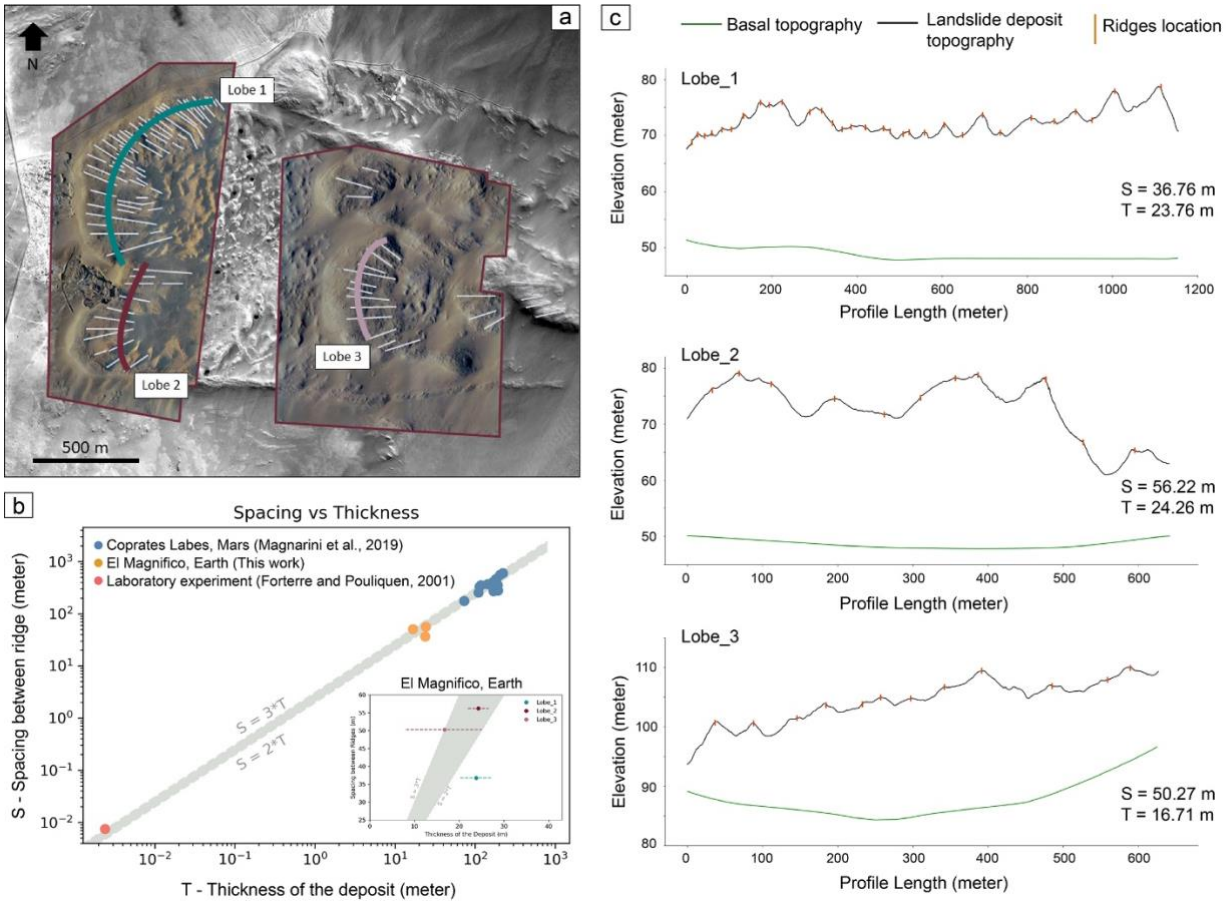

193

194 **Figure 3 – Morphometric analysis.** a) Drone-derived coloured orthoimages within red polygons on satellite-derived black and white
195 orthoimage; white lines represent the location of the crest of the ridges; transversal profiles along which morphometric analysis and
196 deposit thickness calculation are performed for Lobe 1, 2, and 3. b) A plot showing the relationship between the spacing of the ridges
197 and the thickness of the deposit for martian long runout landslide (Magnarini et al., 2019), the El Magnifico landslide on Earth (this
198 current study), and as found in laboratory experiments on rapid granular flows (the data point is extracted from Figure 4a in Forterre
199 and Pouliquen (2001)); the inset shows the scaling relationship calculated at Lobe 1, 2, and 3 in the El Magnifico landslide; the error
200 of the thickness value is derived by combining standard deviation of the elevation variation of the set of profile adjacent to the area
201 of each profile used for the morphometric analysis (Supplementary Material T3 and S6); the grey area represent the range of the
202 scaling relationship found in laboratory experiments on rapid granular flows. c) transversal profiles at Lobe 1, 2, and 3: black lines
203 represent the topographic surface of the deposit extracted from drone-derived digital elevation models; green lines represent the
204 basal surface of the landslide deposit, as inferred by interpolation of topographic contours of the coastal plane (for Lobe 1 and 2;
205 Supplementary Material S6) and by interpolation of topographic contours of the landslide deposit (for Lobe 3, as it stands on Lobe 1
206 and 2; Supplementary Material S6); orange marks represent the location of the crests of the longitudinal ridges.

207

Using drone-derived topography and interpolation-derived basal surface, we also calculated the average thickness of the deposit corresponding to each profile (T in Table 2, Figure 3c; Supplementary Material S6), following the method used in Magnarini et al. (2019). For each profile, we calculated the ratio between the average spacing between the ridges and the average thickness of the landslide deposit (S/T ratio in Table 2). Figure 3b shows the S/T ratio values found at the three profiles. Lobe 2 and Lobe 3 have S/T ratio values of 2.32 and 3, respectively, falling within the range of the scaling relationship between the two parameters found in laboratory experiments on rapid granular flows, which is represented as the grey area in Figure 3b. In contrast, Lobe 1 has S/T ratio value of 1.54, falling outside the range of the scaling relationship.

Table 2 – Morphometric analysis results.

	Profile Length (m)	Number of Ridges	S (m)	T (m)	S/T ratio
Profile Lobe 1	1155	31	36.76	23.76	1.54
Profile Lobe 2	642	11	56.22	24.26	2.32
Profile Lobe 3	628	12	50.27	16.71	3.00

The El Magnifico rock avalanche represents the first morphometric analysis of a terrestrial landslide that shows a clear scaling relationship between the thickness (T) of its deposit and the spacing (S) between its longitudinal ridges (S = 2-3 * T). Until now, this scaling relationship has only been demonstrated at field scale on martian landslides (Magnarini et al., 2019), and for smaller scale ice-free laboratory experiments in rapid granular flows (Forterre and Pouliquen, 2001; Borzsonyi et al., 2009). These results demonstrate that the scaling relationship first suggested by Forterre and Pouliquen (2001): 1) applies over a range of scales; sub-metre-scale (Forterre and Pouliquen, 2001; Borzsonyi et al., 2009), hundreds-of-metre scale (this study), to

tens-of-kilometre-scale (Magnarini et al., 2019); 2) applies for landslides that were not emplaced on ice. The results further support the previous notion that ice is not a necessary condition for the development of longitudinal ridges, indicating the existence of a mechanism that operates across a range of scales during the emplacement of these high-speed events.

5 RELATIONSHIP BETWEEN LONGITUDINAL RIDGES AND INTERNAL STRUCTURES.

The presence of a quarry has exposed a series of outcrops at the terminal part of lobe 2 (Figure 2b). Mather et al. (2014) and Crosta et al. (2017) have exploited the excavation activity of the quarry to observe some internal structures of the landslide deposit. These two works described a ~130m-long and ~20m-high outcrop (see Fig. 6a in Mather et al. (2014) and Fig. 7 in Crosta et al. (2017); blue line in Figure 2b). At the time of our first campaign in 2018, the outcrop had been removed, as the activity of the quarry continued until 2015. Although the quarry was filled with debris, leaving only the top 6-10 m of the landslide deposit uncovered, a ~150m-long uninterrupted section made by excavations with different orientations was available, providing novel longitudinal and transverse segments of the deposit. This provided us with a 3D view of the internal structures within the upper part of the deposit (Figure 2b). Part of the current section intersects a ridge (Figure 2b; outcrops 3, 4, and 5) and it offers an opportunity to interpret the internal structures of the deposit in relation to the ridge. At these locations, we report the presence of several-meters-sized blocks that show preserved original bedding discontinuities (from now on we refer to them as 'megablocks', following the use in Dufresne et al. (2016)). These structures exhibit different degrees of deformation, such as bed thickness reduction and fracturing normal to bedding discontinuities, yet blocks maintain a coherent aspect, that is shattered fragments or sub-blocks do not show displacement relative to each other (Figure 4, Figure 5, Figure 6). The megablocks reported in this study are reminiscent of the 'jigsaw puzzle effect' described by Shreve (1968).

Outcrop 3 (Figure 4) is a longitudinal section of the deposit. A 6 m long and 5 m thick block showing well-preserved original bedding discontinuities which appear within a grey breccia, which is mainly composed of dm-size angular clasts. The bedding discontinuities dip towards the inner part of the deposit with an angle of about 42°. From bottom to top, the beds forming the block decrease in thickness, from about 50 cm to a few centimetres. The thickness reduction seems to be related with thrusting of the upper part that generates a wedge, closing to the top-right of the image. Within the wedge, we observe red layers parallel to the thinned beds (Supplementary Material S7). Similar red layers are seen within the breccia in locations where preserved original bedding are weakly discernible, although not as part of a distinctive block.

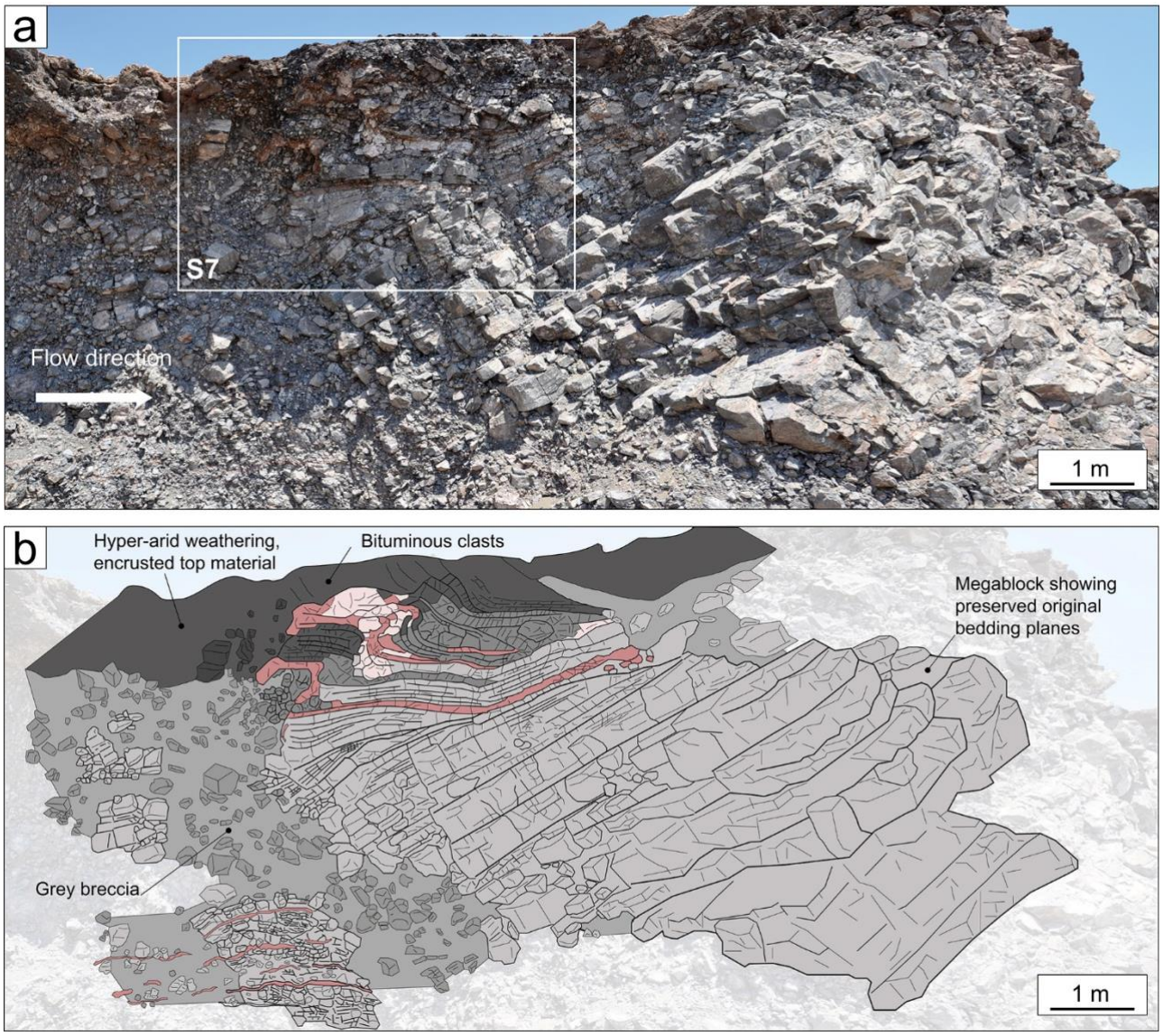

Figure 4 – Outcrop 3. a) Photomosaic of the outcrop 3; S7 is in Supplementary Material. b) schematic representation of the structures observed at the outcrop 3. A megablock about 6 m long and 5 m thick is present within a grey breccia. The megablock shows well-preserved bedding discontinuities. The block is tilted with an angle of about 42°; towards the top of the outcrop, the layers identified by the bedding discontinuities become thinner, closing to the top-right of the image. Close-up view of such wedge generated by thrusting is given in Figure S7 in the Supplementary Material. A smaller, less discernible block with preserved bedding discontinuities is observed near the megablock.

Outcrop 4 (Figure 5) is a transverse section through the deposit. At this location, a megablock about 8 m wide and 7 m high is characterized by the presence of clear layering corresponding to original bedding discontinuities. This megablock emerges within a more typical breccia-type deposit. The preserved bedding

discontinuities have a sub-horizontal apparent attitude. At the upper and left part of this block, planes have dm-spacing. In contrast, at the right-hand side, planes are much more closely spaced to each other, only a few centimetres apart, and at times display more advanced comminution.

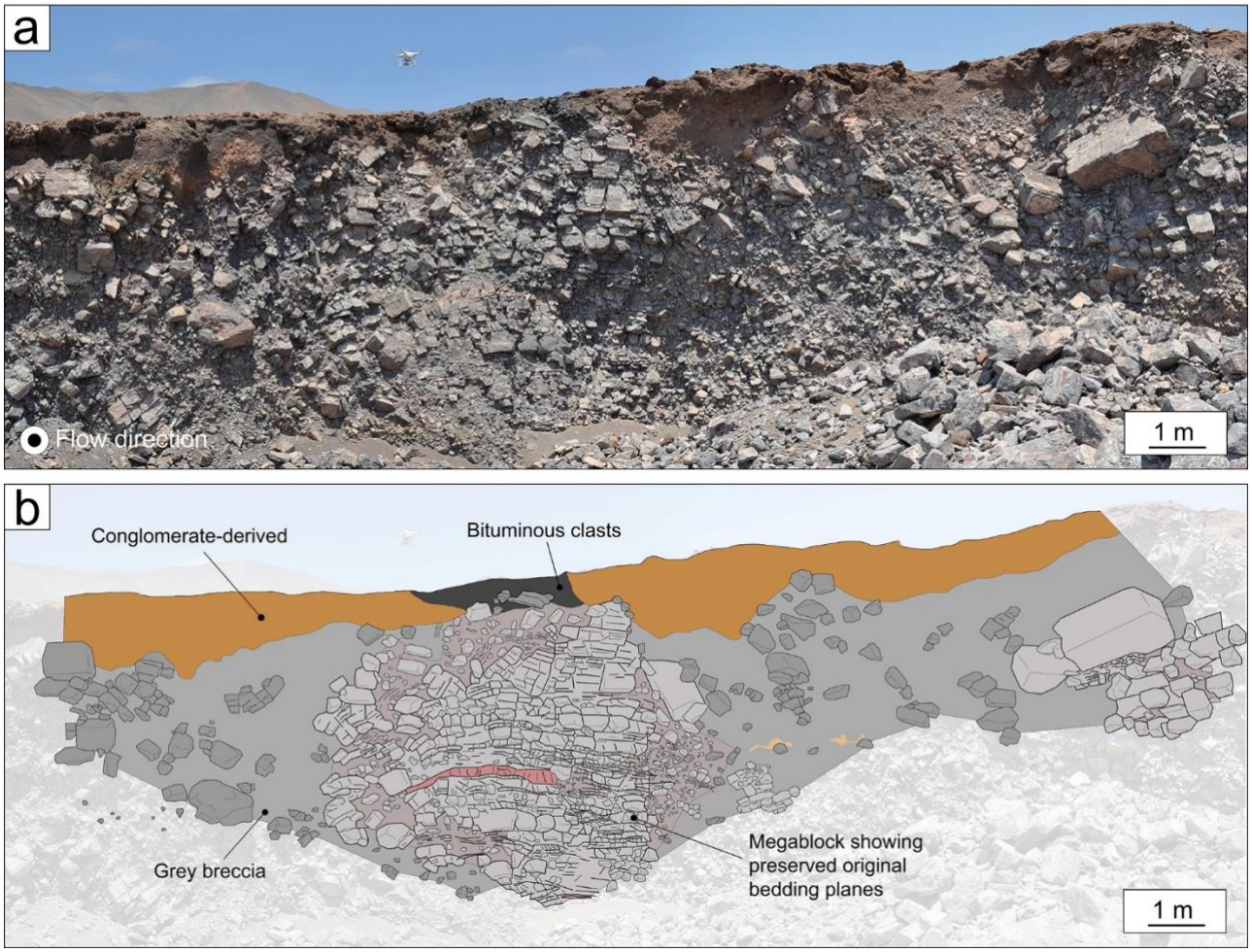

Figure 5 – Outcrop 4. a) Photomosaic of the outcrop 4. b) schematic representation of the structures observed at outcrop 4: at the centre, a megablock about 8 m wide exhibiting well-preserved original bedding discontinuities appears within the breccia; the megablock is capped by dm-size clasts of bituminous sandstones; the breccia is capped by a conglomerate-derived layer that does not exceed 1 m thickness.

Outcrop 5 (Figure 6) is another transverse section of the landslide deposit. Here, we distinguish three megablocks that have the same attitude, 40/38SE. The three megablocks are separated by two bands. The left band is made of clasts with sizes in the range of 5-40 cm. The clasts appear to have the long-axis oriented following the same direction of the bedding discontinuities described earlier. The right band has the same

orientation of the other structures so far described but it is made of smaller clasts, closely packed, which at times give the impression that there is no solution of continuity with the progressively thinner original bedding discontinuities.

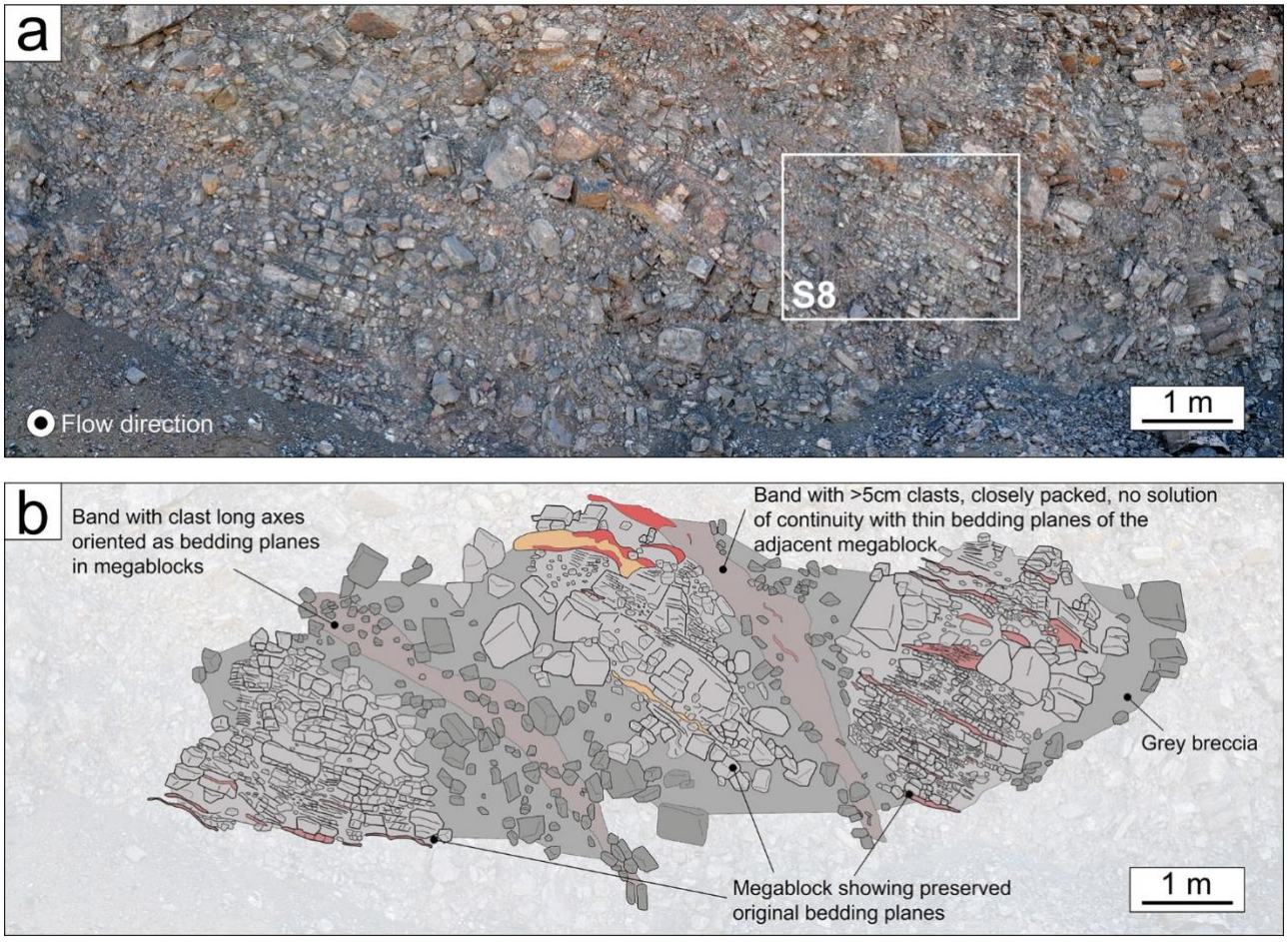

Figure 6 – Outcrop 5. a) Photomosaic of the outcrop (S8 is in Supplementary Material). b) schematic representation of the structures observed at outcrop 5; three areas that exhibit preserved original bedding discontinuities alternate with bands made of smaller clasts oriented as the bedding discontinuities; the band between the middle and right megablock is made of smaller clasts (>5 cm) with same orientation as the other described structures; at times, these clasts show some degree of continuity with the bedding discontinuities of the megablock on the right; the continuity and the high degree of comminution recall a cataclastic aspect.

The megablock at Outcrop 4, located in the central part of the ridge, gently dips inwards (i.e., towards the centre of the deposit, ~ 8°ESE), with a strike perpendicular to the ridge extension. Whereas the megablocks

297 at Outcrop 3 and 5, located at the limbs of the ridge, dip outwards of the ridge structure, 120/42NE and
298 40/38SE, respectively. The attitudes of the megablocks suggest that they are oriented according to their
299 position relative to the ridge, that is the megablocks present an antiform-like arrangement (Figure 7).

300

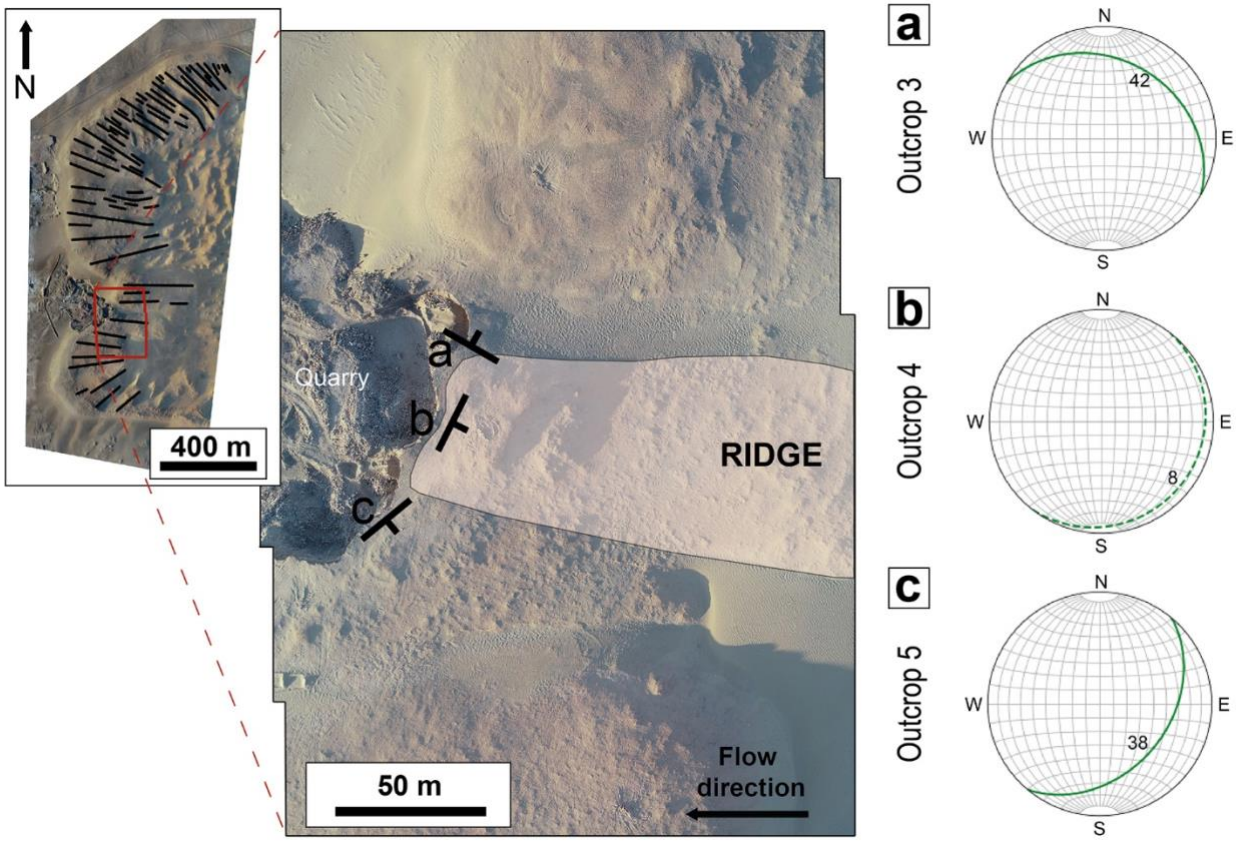

301

302 **Figure 7 – Antiform-like arrangement of megablock.** Orthoimage of the terminal part of the landslide cluster and close-up
303 photomosaic of the quarry; the location of the ridge is represented by the light-coloured area; the orientation of the megablocks
304 observed at outcrops 3, 4 and 5, is shown in the stereonets a), b), and c), respectively.

305

306

6 INTERPRETATION OF THE INTERNAL STRUCTURES AND SEDIMENTOLOGY OF THE DEPOSIT.

The disused quarry at a far end of Lobe 2 is the only location at which the internal structures of the landslide deposit can be examined, therefore our observations are limited to structures at the terminal part of the slide, which may have been affected, if not produced, at the time the landslide came to a halt. Unfortunately, another limitation comes from the fact that the disused quarry is now partially filled with debris produced by the excavation, leaving only the top 6-10 meters of the deposit visible, hence not allowing the observation of the entire deposit section, as instead was possible in the past (see Fig. 6a in Mather et al. (2014) and Fig. 7 in Crosta et al. (2017)). These limitations prevent an exhaustive reconstruction of the sedimentology of the El Magnifico landslide deposit, nevertheless we were able to make several interesting new observations.

6.1 STRESS FLUCTUATIONS DURING EMPLACEMENT.

The presence of megablocks at the distal part of the landslide deposit calls into question the idea of progressive facies maturation with distance that was suggested to occur in some cases (Dufresne et al., 2016). Their presence within a breccia may result from heterogeneous stress distribution within the sliding mass and through the entire runout, allowing the preservation of a large portion of the original slope-forming material. Large fluctuation of stresses are reported in computer simulations by Campbell et al. (1995) and Johnson et al. (2016), and they are considered the hallmark of the acoustic fluidization hypothesis (Melosh, 1979). The preservation of megablocks at around 4 km away from the slide head scarp can be plausibly associated with the existence of stress fluctuation within the sliding mass.

6.2 LACK OF TURBULENCE DURING EMPLACEMENT.

At Outcrop 1 (Figure 8) and Outcrop 2 (Figure 9), we see well-defined contacts between two different lithologies (conglomerates and breccia), which do not intermix. At the upper part of the outcrop 1, a

longitudinal section of the landslide deposit, the contact is sub-horizontal, with conglomerate-derived layer above the grey breccia. The upper part of the breccia is comprised of large (8 to 50 cm) angular to sub-rounded clasts, with the largest clasts found close to the contact with the above conglomerate-derived-layer. At one location, the clasts inject into the layer above. At the lower left of the outcrop, conglomerate-derived material appears also within the grey breccia and the contact is still well-defined (Supplementary Material S9). Around the left corner of the outcrop, we were able to follow the conglomerate-derived material and the observations suggest an interdigitating relationship along a transversal view point (Supplementary Material S10). At outcrop 2, a transverse section of the landslide deposit, the contact between the conglomerate-derived material and the breccia occurs both sub-horizontally and sub-vertically. At the section, we observe the grey breccia both underlying and laterally bounding the conglomerate-derived material.

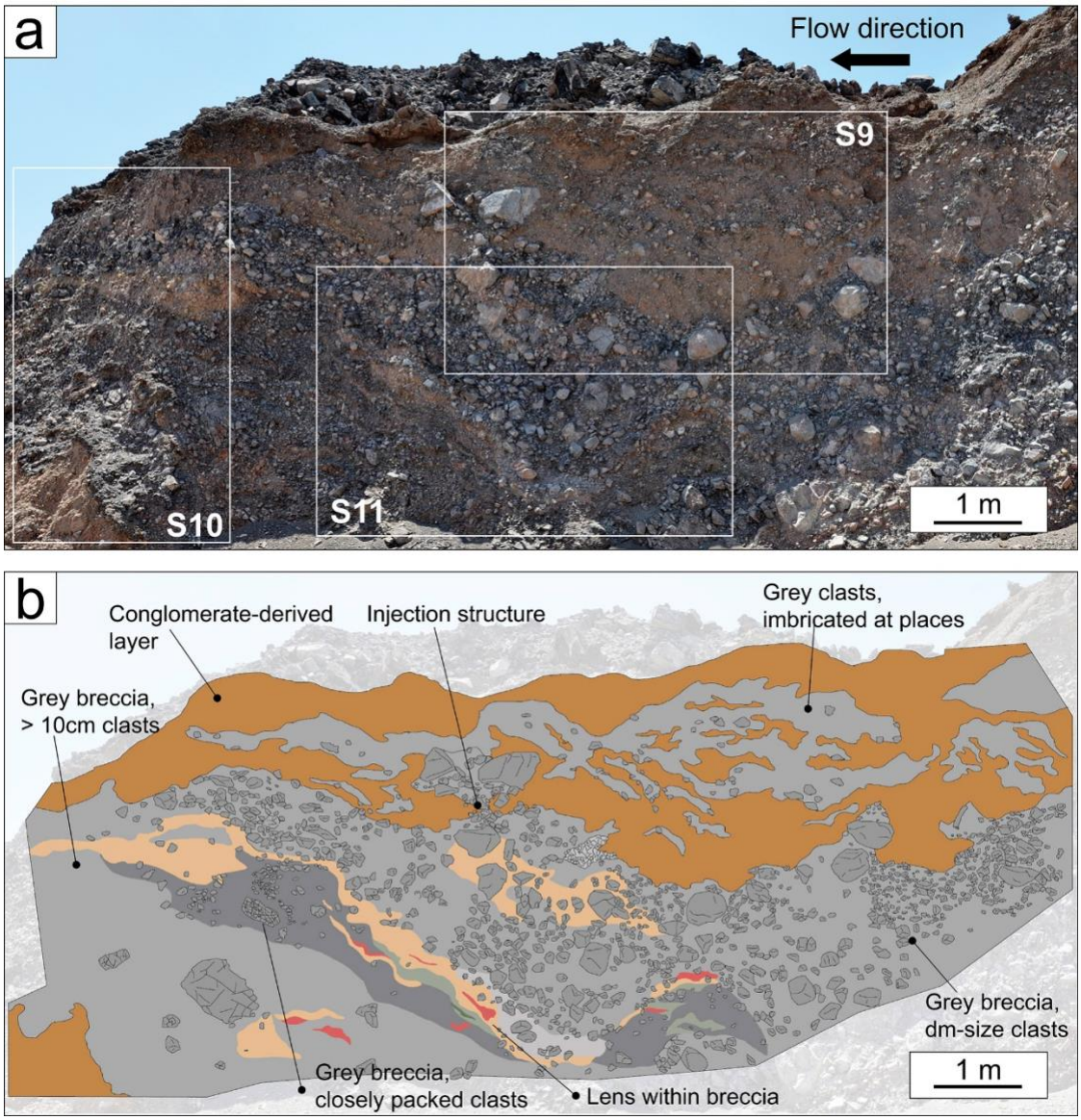

343

344 **Figure 8 – Outcrop 1.** a) Photomosaic of the outcrop (S9, S10, S11 are in Supplementary Material). b) schematic representation of

345 the lithologies and structures observed: two main layers are recognizable: a top matrix-supported, brown layer and a bottom grey,

346 clast-supported breccia, with larger clasts in the upper part, within which a red-yellow-green lens appear.

347

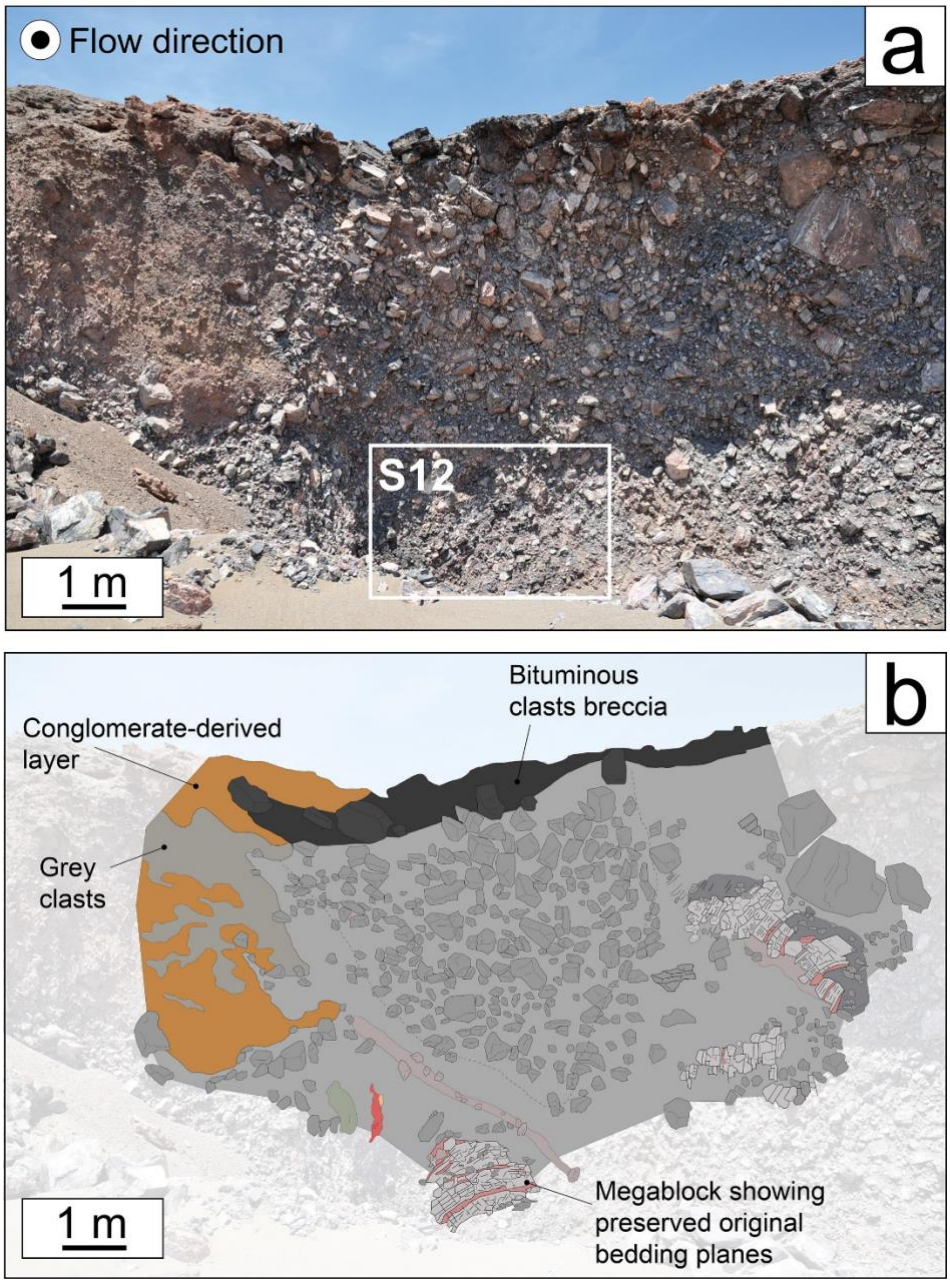

348

349 **Figure 9 – Outcrop 2.** a) Photo of the outcrop, in which a lateral transition from the brown, matrix-supported layer to the grey, clast-
350 supported breccia is visible; (S12 is in Supplementary Material). b) schematic representation of the outcrop 2 that highlights the
351 structures observed: to the left, the lateral contact between the conglomerate-derived layer and the grey breccia; at the bottom and
352 to the right, blocks that show preserved original bedding discontinuities are present within the grey breccia; in the centre, a roughly
353 v-shaped area characterized by angular blocks densely packed with an apparent inverse grading is seen.

354

355

356 The observation of well-defined contacts between different lithologies within the landslide deposit are in line
357 with the classical inference of lack of chaotic mixing of the landslide debris during emplacement (e.g., Shreve,
358 1968; Dufresne et al., 2016 and reference within). The preservation of the source stratigraphy is recurrently
359 reported in the literature and the fact that we observe conglomerates at the top at Outcrop 1 (which is the
360 lithology at the top of the stratigraphic sequence at the scarp, Figure 1d) may suggest that this is also the
361 case for the El Magnifico landslide. However, the lateral contact between the conglomerates and the breccia,
362 seen at Outcrop 2, and the seemingly interdigitating relationship between the two lithologies in Outcrop 1
363 suggest a more complex level of interaction during landslide emplacement. These observations do not
364 support the notion of a carapace made of angular clasts riding atop a shearing body, which has been used to
365 represent typical rock avalanche and rock slide facies and features (Weidinger et al., 2014; Dufresne et al.,
366 2016). Similarly, these observations do not fit with the idea that long runout landslides move as a solid block
367 with shearing restricted to the basal region. This latter view has been challenged by Campbell et al. (1995),
368 who showed, using 2D computer simulations, that the landslide is characterized by distributed shearing. In
369 fact, we note similarity between some of the observed types of contacts and structures at the El Magnifico
370 landslide, and in the computer simulations by Campbell et al. (1995), such as an interdigitating relationship
371 between the strata (see Plate 3 in Campbell et al. (1995) and S10 in Supplementary Material). As affirmed by
372 Johnson et al. (2016), three-dimensional computer simulations would be highly desirable; in addition to
373 providing a further level of comparison for field-based observations, they would also provide insights on the
374 importance of the three-dimensional effects of the mechanisms proposed for the formation of longitudinal
375 ridges in long runout landslides.

376

377 # 7 DISCUSSION.

378 Magnarini et al. (2019) proposed that longitudinal ridges in a martian long runout landslide developed from
379 a convection-style motion that derives from the physics of rapid granular flows (Forterre and Pouliquen,
380 2001). This conclusion was based on the finding of the same scaling for the ratio of longitudinal ridges spacing

and the thickness of the landslide at both the martian slide and the ice-free laboratory experiments of rapid granular flows (Forterre and Pouliquen, 2001; Borzsonyi et al., 2009). Here we report that the same scaling relationship is found in the terrestrial El Magnifico landslide. This has two important implications for the emplacement mechanism: firstly, it suggests that whatever is the mechanism for the formation of the longitudinal ridges, it can operate over 5 orders of magnitude (Figure 3b); secondly, the mechanism is likely environment-independent, in support of the conclusion that ice is not a necessary condition for the formation of longitudinal ridges.

Despite these intriguing implications, conclusive evidence for the mechanism responsible for the formation of longitudinal ridges at the field scale remains elusive. For that reason, direct observations of terrestrial long runout landslide deposits are fundamental in order to try and link laboratory-scale models to field-scale natural long runout landslides. The quarry excavation at the El Magnifico landslide that transversally intersects a longitudinal ridge provides an unprecedented opportunity to search for evidence of the convection-style mechanism described for the physics of rapid granular flows and suggested for the formation of longitudinal ridges in a martian long runout landslide. In order to assess a possible emplacement mechanism and drawing upon the existence of the scale- and environment- independent scaling between the ridge spacing and the deposit thickness, we turn to discuss the relationship between the longitudinal ridges and internal structures, and the evidence of stress fluctuations and lack of turbulence.

7.1 IMPLICATIONS FOR EMPLACEMENT MECHANISM.

The observed organization of the megablocks seemingly relative to the presence of a ridge does not necessarily support a convective-style motion, as suggested by Magnarini et al. (2019) in their study of a martian long runout landslide. Although the antiform-like arrangement of the megablock may represent a frame of a convective mechanism scenario (Figure 10d), the fact that we do report evidence of lack of turbulence (see Outcrop 1 and Outcrop 2) suggests that this type of mechanism may not have developed during emplacement of the El Magnifico landslide. Incorporating the observation from Mather et al. (2014) and Crosta et al. (2017) of an undulated colourful layer within the breccia exhibiting kink folds, we suggest

that the observed antiform-like arrangement of the megablocks may reflect a deformation induced by a vibrational mode operating within the slide (Figure 10c).

The ambiguity of the interpretation of the internal structures raises the question of whether the mechanical instability, responsible for the formation of longitudinal ridges observed at laboratory scale in rapid granular flows (Forterre and Pouliquen, 2001; Borzsonyi et al., 2009), actually occurs at the field scale in long runout landslides. If a different style of motion had indeed operated in the El Magnifico landslide, it is interesting that regardless of how the mechanism involved operates, the same scaling relationship between the wavelength of the ridges and the thickness of the deposit recurs and the reason for this may lie in the existence of some degree of universality in the mechanism of longitudinal ridge pattern-formation.

As it is understood from laboratory experience (Aranson and Tsimring, 2009), pattern-formation mechanisms within a granular medium can arise from injection of energy through vibrations, either through the interaction between the roughness of a surface and the grains of a high-speed flow or through vibrations transmitted to a granular layer resting on a plate. At the field scale, ground vibrations are generated during landslide events and their occurrence is reveal through seismic signals (e.g., Hibert et al., 2017; Dufresne et al., 2019). Although so far, no attempt has ever been made to associate the dominant frequencies of such vibrations to neither the prediction of acoustic fluidization nor to surficial pattern formation, acoustic waves are expected to be generated during every landslide event and to propagate through the sliding mass. We expect that vibrations are not only provided through ground vibrations generated by the event itself, but also through the interaction between the sliding mass and the roughness of the surface over which it moves, as shown from laboratory experience. Therefore, it is plausible to conceive vibrations as the fundamental way through which energy is supplied to the landslide-system.

We conceptualize the occurrence of a vibrated-assisted mechanism and a convection-type mechanism as a continuum that is dependent on both the lithologies involved, the duration of the event and the velocity (i.e., energy) at play. Critically, both mechanisms rely on the same type of energy input, vibrations. A mechanical instability would emerge generating a convection-style of motion when conditions of certain lithologies, velocity and stresses brecciate the sliding mass to the point that it behaves in the manner of a granular flow.

In some cases, such as the El Magnifico landslide, this extreme mechanical instability may not emerge and pattern-forming vibration within the sliding mass may, in this case, dominate.

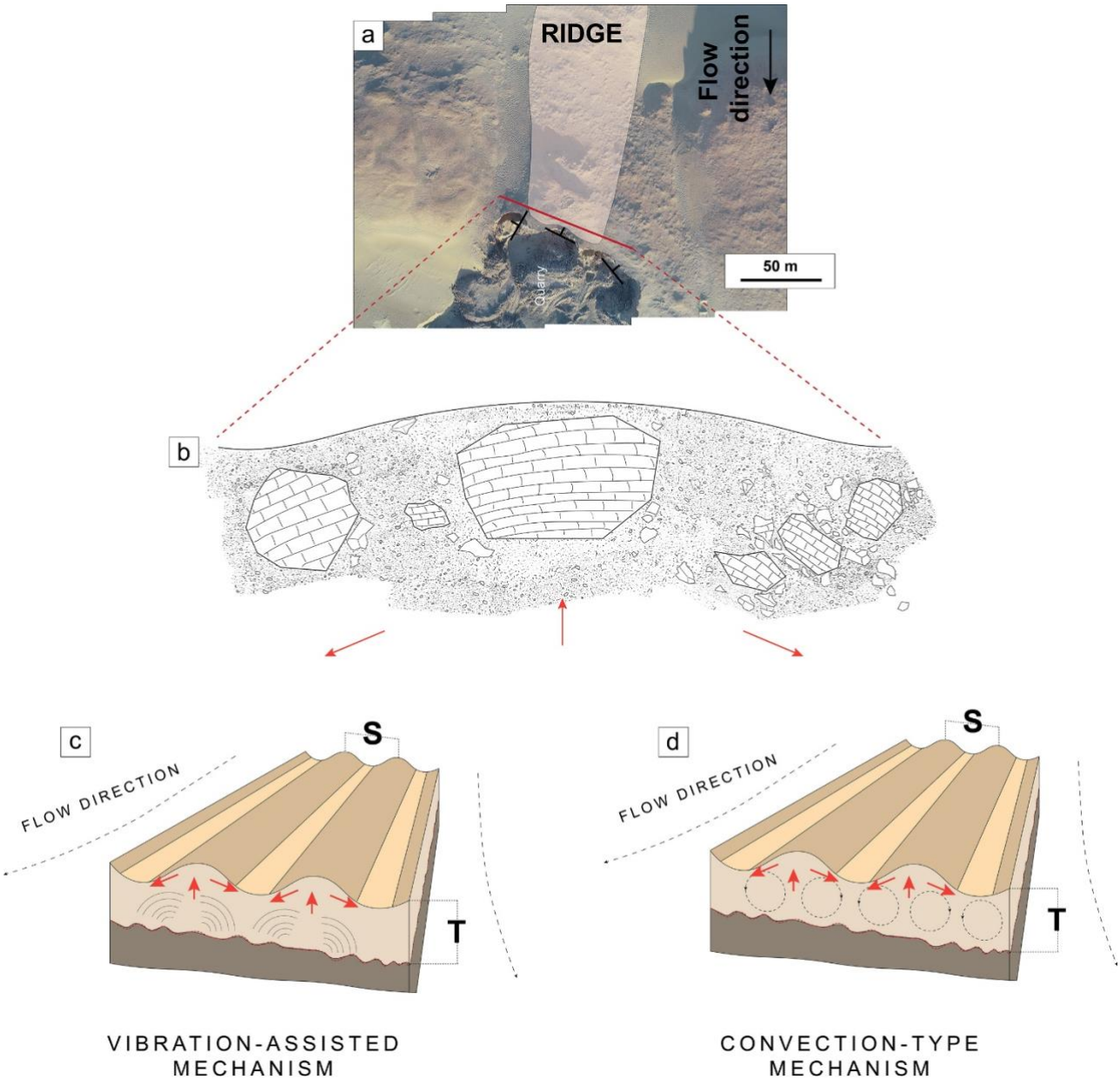

Figure 10 – Longitudinal pattern-forming mechanisms. a) Top-view photomosaic of the ridge cut by the quarry where internal structures of the landslide deposit were observed; red line corresponds to the profile at which the internal structures observed are schematically represented in b). b) Schematic representation of the megablocks relative to the ridge; the red arrows represent the direction of the internal antiform-like deformation; the red arrows represent the sense of the internal deformation. c) Model of longitudinal ridge formation from internal deformation of the sliding mass due to the existence of pattern-forming vibrations. d) Model of longitudinal ridge formation from convection-cells within the sliding mass due to the rise of a mechanical instability.

8 CONCLUSIONS.

For the first time in terrestrial long runout landslides, we report the occurrence of a scaling relationship between the wavelength of longitudinal ridges and the thickness of a 4-km-long landslide deposit. This scaling relationship is in agreement with previous results of both ice-free laboratory experiments on rapid granular flows (~1 m in length) and a martian long runout landslide (~60 km in length). The scaling relationship found suggests that, whatever the formation mechanism, their formation mechanism can operate over 5 orders of magnitude (Figure 3b). The recurrence across scales of the same scaling relationship between the wavelength of the longitudinal ridges and the thickness of the deposit strongly suggests the existence of a scale-independent mechanism that takes place during the emplacement of these high-speed events. Moreover, our new discovery of the applicability of this scaling relationship to the El Magnifico landslide in the Atacama region, where ice was certainly not present at the time of the landslide emplacement, further supports the hypothesis that ice is not a necessary condition for the development of longitudinal ridges.

In order to ground truth the convection-style mechanism proposed for the formation of longitudinal ridges in a martian landslide (Magnarini et al., 2019), we explored a transverse section of one of the longitudinal ridges of the terrestrial El Magnifico landslide. We do not find unequivocal evidence in support of a convection-style mechanism. Instead, evidence of stress fluctuations, which were suggested to be associated with acoustic fluidization, and the antiform-like arrangement of the internal structures of the deposit led us to speculate on the existence of an alternative vibration-assisted mechanism.

The novel observations on the relationship between longitudinal ridges and the internal structures within the landslide deposit presented in our study provide new elements to the discussion about the formation mechanism of longitudinal ridges and the interpretation of similar features on Earth and on Mars. The understanding of the formation mechanism of longitudinal ridges and the mechanics of long runout landslides will further benefit from experimental and theoretical work that aims to explore the effect of acoustic waves that propagate through the sliding mass.

AUTHOR CONTRIBUTIONS.

G.M., T.M.M.: Conceptualization; G.M.: Writing – Original Draft; T.M.M., L.G., P.M.G., J.B.: Writing – Review and Editing; G.M., T.M.M., J.B.: conducted field work; G.M.: created drone-derived dataset; P.M.G.: created satellite-derived dataset;

ACKOWLEDGMENTS.

G.M. and T.M.M. acknowledge Science and Technology Facilities Council (STFC) funding ST/N504476/1. G.M. and J.B are grateful to Mr. Alfredo of the San Marco Mine and Mr. Bernardo of the Los Verdes Shooting Range for the precious help in the field.

This work was supported by public funds received in the framework of GEOSUD, a project (ANR-10-EQPX-20) of the program "Investissements d'Avenir" managed by the French National Research Agency". We thank DataTerra DINAMIS, the French Space Agency CNES and their ISIS programme for access to the Pléiades data. We are grateful to Susan Conway for kindly requesting and sharing Pléiades data.

REFERENCES.

Allmendinger, R.W., González, G., 2010. Invited review paper: Neogene to Quaternary tectonics of the coastal Cordillera, northern Chile. Tectonophysics 495, 93-110.

Amundson, R., Dietrich, W., Bellugi, D., Ewing, S., Nishiizumi, K., Chong, G., Owen, J., Finkel, R., Heimsath, A., Stewart, B., Caffee, M., 2012. Geomorphologic evidence for the late Pliocene onset of hyperaridity in the Atacama Desert. Geological Society of America Bulletin 124, 1048-1070.

Aranson, I.S., Tsimring, L., 2009. Granular patterns /by Igor S. Aranson, Lev T͡Simring. Oxford : Oxford University Press, Oxford.

Beddingfield, C.B., Beyer, R.A., Singer, K.N., McKinnon, W.B., Runyon, K., Grundy, W., Stern, S.A., Bray, V., Dhingra, R., Moore, J.M., Ennico, K., Olkin, C.B., Schenk, P., Spencer, J.R., Weaver, H.A., Young, L.A., 2019. Landslides on Charon. Icarus.

Borzsonyi, T., Ecke, R.E., McElwaine, J.N., 2009. Patterns in Flowing Sand: Understanding the Physics of Granular Flow. Phys Rev Lett 103.

Boyce, J.M., Mouginis-Mark, P.J., Robinson, M., 2020. The Tsiolkovskiy crater landslide, the moon: An LROC view. Icarus 337, 113464.

Campbell, C.S., Cleary, P.W., Hopkins, M., 1995. Large-scale landslide simulations: Global deformation, velocities and basal friction. Journal of Geophysical Research: Solid Earth 100, 8267-8283.

Collins, G.S., Melosh, H.J., 2003. Acoustic fluidization and the extraordinary mobility of sturzstroms. J Geophys Res-Sol Ea 108.

Conway, S.J., Balme, M.R., 2014. Decameter thick remnant glacial ice deposits on Mars. Geophys Res Lett 41, 5402-5409.

Crosta, G.B., Frattini, P., Valbuzzi, E., De Blasio, F.V., 2018. Introducing a New Inventory of Large Martian Landslides. Earth and Space Science 5, 89-119.

Crosta, G.B., Hermanns, R.L., Dehls, J., Lari, S., Sepulveda, S., 2017. Rock avalanches clusters along the northern Chile coastal scarp. Geomorphology 289, 27-43.

Davies, T.R., 1982. Spreading of Rock Avalanche Debris by Mechanical Fluidization. Rock Mechanics 15, 9-24.

Davies, T.R., McSaveney, M.J., 2009. The role of rock fragmentation in the motion of large landslides. Eng Geol 109, 67-79.

De Blasio, F.V., 2011. Landslides in Valles Marineris (Mars): A possible role of basal lubrication by sub-surface ice. Planet Space Sci 59, 1384-1392.

Dufresne, A., Bosmeier, A., Prager, C., 2016. Sedimentology of rock avalanche deposits - Case study and review. Earth-Sci Rev 163, 234-259.

Dufresne, A., Davies, T.R., 2009. Longitudinal ridges in mass movement deposits. Geomorphology 105, 171-181.

Dufresne, A., Wolken, G.J., Hibert, C., Bessette-Kirton, E.K., Coe, J.A., Geertsema, M., Ekström, G., 2019. The 2016 Lamplugh rock avalanche, Alaska: deposit structures and emplacement dynamics. Landslides.

Erismann, T.H., Heuberger, H., Preuss, E., 1977. Fused Rock of Kofels (Tyrol) - Frictionite Generated by a Landslide. Tscher Miner Petrog 24, 67-119.

Evenstar, L.A., Mather, A.E., Hartley, A.J., Stuart, F.M., Sparks, R.S.J., Cooper, F.J., 2017. Geomorphology on geologic timescales: Evolution of the late Cenozoic Pacific paleosurface in Northern Chile and Southern Peru. Earth-Sci Rev 171, 1-27.

Forterre, Y., Pouliquen, O., 2001. Longitudinal vortices in granular flows. Phys Rev Lett 86, 5886-5889.

Goren, L., Aharonov, E., 2007. Long runout landslides: The role of frictional heating and hydraulic diffusivity. Geophys Res Lett 34.

Goren, L., Aharonov, E., Anders, M.H., 2010. The long runout of the Heart Mountain landslide: Heating, pressurization, and carbonate decomposition. J Geophys Res-Sol Ea 115.

Hibert, C., Ekström, G., Stark, C.P., 2017. The relationship between bulk-mass momentum and short-period seismic radiation in catastrophic landslides. Journal of Geophysical Research: Earth Surface 122, 1201-1215.

Howard, K.A., 1973. Avalanche Mode of Motion - Implications from Lunar Examples. Science 180, 1052-1055.

Hu, W., Huang, R.Q., McSaveney, M., Zhang, X.H., Yao, L., Shimamoto, T., 2018. Mineral changes quantify frictional heating during a large low-friction landslide. Geology 46, 223-226.

Johnson, B.C., Campbell, C.S., Melosh, H.J., 2016. The reduction of friction in long runout landslides as an emergent phenomenon. J Geophys Res-Earth 121, 881-889.

Legros, F., Cantagrel, J.M., Devouard, B., 2000. Pseudotachylyte (Frictionite) at the Base of the Arequipa Volcanic Landslide Deposit (Peru): Implications for Emplacement Mechanisms. The Journal of Geology 108, 601-611.

Lucchitta, B.K., 1979. Landslides in Valles Marineris, Mars. J Geophys Res 84, 8097-8113.

Magnarini, G., Mitchell, T.M., Grindrod, P.M., Goren, L., Schmitt, H.H., 2019. Longitudinal ridges imparted by high-speed granular flow mechanisms in martian landslides. Nature Communications 10, 4711.

Mather, A.E., Hartley, A.J., Griffiths, J.S., 2014. The giant coastal landslides of Northern Chile: Tectonic and climate interactions on a classic convergent plate margin. Earth Planet Sc Lett 388, 249-256.

Melosh, H.J., 1979. Acoustic Fluidization - New Geologic Process. J Geophys Res 84, 7513-7520.

Mitchell, T.M., Smith, S.A.F., Anders, M.H., Di Toro, G., Nielsen, S., Cavallo, A., Beard, A.D., 2015. Catastrophic emplacement of giant landslides aided by thermal decomposition: Heart Mountain, Wyoming. Earth Planet Sc Lett 411, 199-207.

Novoa, A.T., 1970. Carta Geologica de Chile: Cuagrangulos Iquique y Caleta Molle: Provincia de Tarapaca. Instituto de Investigaciones Geologicas (Chile). Carta Geologica N. 21 y 22.

Paguican, E.M.R., de Vries, B.V., Lagmay, A.M.F., 2014. Hummocks: how they form and how they evolve in rockslide-debris avalanches. Landslides 11, 67-80.

Quantin, C., Allemand, P., Delacourt, C., 2004a. Morphology and geometry of Valles Marineris landslides. Planet Space Sci 52, 1011-1022.

Quantin, C., Allemand, P., Mangold, N., Delacourt, C., 2004b. Ages of Valles Marineris (Mars) landslides and implications for canyon history. Icarus 172, 555-572.

Schmidt, B.E., Hughson, K.H.G., Chilton, H.T., Scully, J.E.C., Platz, T., Nathues, A., Sizemore, H., Bland, M.T., Byrne, S., Marchi, S., O'Brien, D.P., Schorghofer, N., Hiesinger, H., Jaumann, R., Pasckert, J.H., Lawrence, J.D., Buzckowski, D., Castillo-Rogez, J.C., Sykes, M.V., Schenk, P.M., DeSanctis, M.C., Mitri, G., Formisano, M., Li, J.Y., Reddy, V., LeCorre, L., Russell, C.T., Raymond, C.A., 2017. Geomorphological evidence for ground ice on dwarf planet Ceres. Nat Geosci 10, 338-343.

565 Shea, T., van Wyk de Vries, B., 2008. Structural analysis and analogue modelling of the kinematics and
566 dynamics of large-scale rock avalanches. Geosphere 4, 657-686.
567 Shreve, R.L., 1968. The Blackhawk Landslide, in: Shreve, R.L. (Ed.), The Blackhawk Landslide. Geological
568 Society of America.
569 Singer, K.N., McKinnon, W.B., Schenk, P.M., Moore, J.M., 2012. Massive ice avalanches on Iapetus
570 mobilized by friction reduction during flash heating. Nat Geosci 5, 574-578.
571 Vardoulakis, I., 2000. Catastrophic landslides due to frictional heating of the failure plane. Mech Cohes-
572 Frict Mat 5, 443-467.
573 Voight, B., Faust, C., 1982. Frictional Heat and Strength Loss in Some Rapid Landslides. Geotechnique 32,
574 43-54.
575 Weidinger, J.T., Korup, O., Munack, H., Altenberger, U., Dunning, S.A., Tippelt, G., Lottermoser, W., 2014.
576 Giant rockslides from the inside. Earth Planet Sc Lett 389, 62-73.

577